ChemComm

COMMUNICATION

View Article Online
View Journal | View Issue

Cite this: *Chem. Commun.*, 2021, **57**, 2265

Received 3rd December 2020,
Accepted 22nd January 2021

DOI: 10.1039/d0cc07867k

rsc.li/chemcomm

Purine-based Ir(III) complexes for sensing viscosity of endo-plasmic reticulum with fluorescence lifetime imaging microscopy†

Xin Liu, Kun Li, * Lei Shi, Hong Zhang, Yan-Hong Liu, Hao-Yuan Wang, Nan Wang and Xiao-Qi Yu *

Novel purine-based iridium complexes were designed for selective determination of ER viscosity. The Ir-PH possessed excellent ER targeting ability and could distinguish the viscosity changes under ER stress by fluorescence lifetime image microscopy (FLIM), which may accelerate the development of relative quantitative detection of microenvironment changes at the subcellular level.

Intracellular viscosity is closely linked to cellular processes, such as transportation, diffusion, and metabolism.[1] Therefore, it is of great significance that tracking intracellular viscosity changes can help us to understand the physiological or pathological processes of cells.[2,3] The endoplasmic reticulum (ER) is an important organelle, which is mainly responsible for Ca^{2+} storage, protein synthesis and transportion.[4] The accumulation of unfolded or excessive misfolded proteins will disturb the regular function of ER and it may lead to ER stress; which may eventually lead to some kinds of diseases, including Alzheimer's disease, obesity or diabetes and cancers.[5,6] Meanwhile, the accumulation of these unfolded or misfolded proteins would certainly change the viscosity of the ER;[6] so it is valuable to develop probes to detect the viscosity changes of ER during ER stress.

Fluorescent chemosensors have been extensively developed in the last 10 years, and have provided a good method for tracking small molecules or microenvironmental changes within living cells.[7–12] However, as traditional fluorescence-intensity-based probes, we may not completely avoid the influence of concentration. FLIM is based on a natural property and could solve the problem,[13] which is often closely related to the environment, such as temperature, dielectric constant, and viscosity.[14] Combined with existing reports, many diseases are associated with the cellular microenvironment. Therefore, FLIM would be highly promising for studying alterations in the cellular microenvironment.

Recently, iridium(III) complexes have been widely investigated in oxygen sensors,[15] photodynamic therapy (PDT),[16–18] and bioimaging because of their excellent large Stokes shift, long luminescence lifetime and high quantum yield. Disappointedly, lots of reported iridium(III) ligands often regulate obvious cytotoxicity.[19,20] Purine that is present in biological molecules has been used as anticancer agents, antiviral drugs and receptor antagonists due to its biological importance.[21–23] Although the structure of purines contains N atoms and conjugated planes, few studies have applied it to the construction of fluorescent probes. Furthermore, purine has not been used to construct ligands to synthesise iridium(III) complexes until now. In our previous work, purine was utilized as the core structure to build a series of AIE fluorophores performing an excellent effect in cell imaging with good biocompatibility.[24–26] This also makes it possible for us to synthesize iridium(III) complexes for cell imaging.

On the other hand, the reported iridium(III) complexes for sensing viscosity were designed with a rotatable bond or by adding a rotor, such as **Ir6**,[13] **1**,[27] and **C10**[28] (Scheme 1). Due to the introduction of freely rotating rotors or bonds, a problem is that it would reduce the conjugation of the entire compound, and cause large energy dissipation, resulting in intense responses to subtle changes. Therefore, it is urgent to develop a new strategy to solve this problem.

In the present study, we introduce purine derivatives into the iridium(III) complex **Ir-PH** for the first time, which can aggregate in ER owing to its lipophilic and cationic characteristics. This complex could possess viscosity-sensitive properties without a plane or bond that could rotate individually. We speculated that the reason for viscosity response may be the changes of torsion angles between the phenyl ring and purine, and between the pyridine ring and β-carboline; so we designed **Ir-PMe-1** and **Ir-PMe-2** to confirm our conjecture. We deduced that **Ir-PMe-1** had a weaker

Key Laboratory of Green Chemistry and Technology, Ministry of Education, College of Chemistry, Sichuan University, Chengdu, 610064, China.
E-mail: kli@scu.edu.cn, xqyu@scu.edu.cn

† Electronic supplementary information (ESI) available: Synthetic schemes, experimental procedures, characterization of all compounds, and supplementary data. CCDC 2014009 and 2014010. For ESI and crystallographic data in CIF or other electronic format see DOI: 10.1039/d0cc07867k

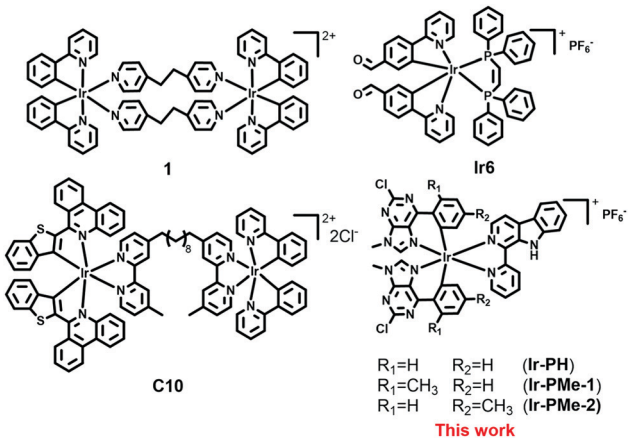

Scheme 1 Chemical structures of iridium(III) complexes for sensing viscosity.

viscosity response and **Ir-PMe-2** was consistent with **Ir-PH**, because the methyl of **Ir-PMe-1** would restrict the change of torsion angles between the phenyl ring and purine. Actually, the experimental results were consistent with our conjecture. We confirmed that **Ir-PH** could localize to ER and **Ir-PH** could reflect the viscosity of dysfunctional ER using FLIM. In conclusion, our work demonstrates the potential of revealing microenvironmental changes at the subcellular level.

The synthetic routes for **Ir-PH**, **Ir-PMe-1** and **Ir-PMe-2** are shown in the ESI,† (Scheme S1). **Ir-PH** is also characterized by X-ray crystal diffraction analysis (Fig. 1C and Fig. S1, Tables S1, S2, ESI†). We systematically studied the photophysical properties of **Ir-PH**, **Ir-PMe-1** and **Ir-PMe-2** (Table S3, ESI†). In PBS at 298 K, they showed intense absorption bands at 270–360 nm assigned to spin-allowed intraligand (^{1}IL) transitions and less intense absorption bands at 360–500 nm assigned to a mixture of spin-allowed and spin-forbidden metal-to-ligand charge transfer transitions (^{1}MLCT/^{3}MLCT) (Fig. S2, ESI†).[29] Upon excitation at 370 nm, **Ir-PH** and **Ir-PMe-2** display strong emission at *ca.* 550 nm, and **Ir-PMe-1** has a 20 nm red shift and exhibits weaker emission compared with **Ir-PH**. This phenomenon confirmed our conjecture that the methyl of **Ir-PMe-1** restricted the change of torsion angles between the phenyl ring and purine and led to an increased degree of conjugation.

We firstly investigated the fluorescence spectra of all complexes in various solvents. The results revealed that **Ir-PH** and **Ir-PMe-2** had much stronger fluorescence intensity in 99% glycerol than other solvents, while for **Ir-PMe-1** it was not obvious. As we know, glycerol–water mixtures are frequently used to adjust the viscosity of a solution. To investigate the influence of viscosity on the emission intensity of all complexes, fluorescence spectra were recorded in a series of viscosity gradient mixtures composed of glycerol and water at room temperature. As shown in Fig. 2, **Ir-PH** exhibited very weak fluorescence in low viscosity, while increasing the proportion of glycerol, the fluorescence intensity of **Ir-PH** enhanced dramatically and increased 22.6-fold at 550 nm as the viscosity increases from 1.01 cP to 76.78 cP, which could be easily observed by the naked eye. A linear correlation was obtained between emission intensity and solvent viscosity. **Ir-PMe-1** emission was enhanced 11.8-fold at 570 nm (Fig. S5, ESI†) and **Ir-PMe-2** was enhanced by 37.5-fold at 550 nm (Fig. S6, ESI†). This conclusion

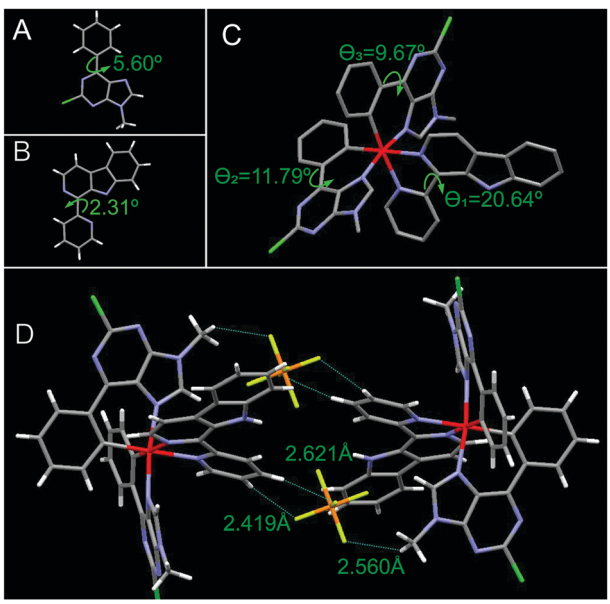

Fig. 1 (A) The single crystal structure of compound **PH**; (B) the single crystal structure of **1-Py-βC**;[29] (C) the single crystal structure of **Ir-PH**, the H atoms, counterions, and solvent have been omitted for clarity; (D) the molecular packing of **Ir-PH**. Carbon, hydrogen, nitrogen and iridium atoms are shown in grey, white, blue, and red, respectively.

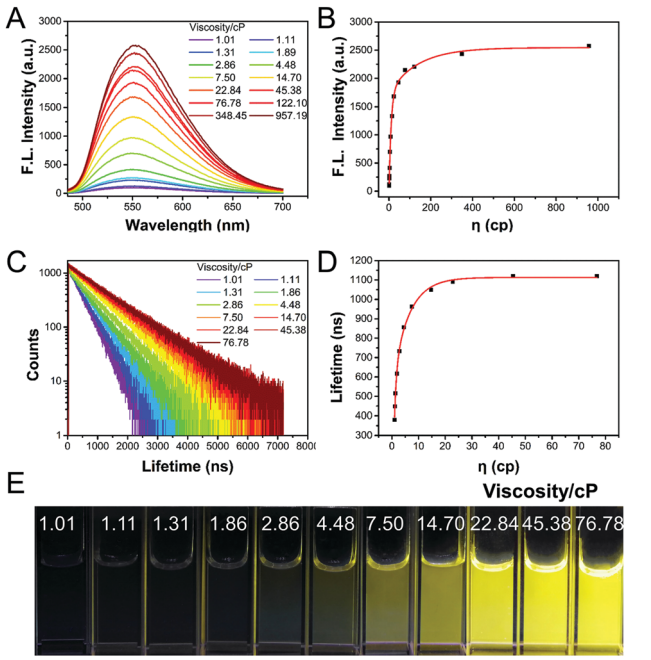

Fig. 2 (A) Fluorescence emission intensities and (C) lifetimes of **Ir-PH** (10 μM) in mixtures of water and glycerol at different viscosities (1.01, 1.11, 1.31, 1.86, 2.86, 4.48, 7.50, 14.70, 22.84, 45.38, and 76.78 cP); (B) fluorescence emission intensity–viscosity curves; (D) fluorescence lifetime–viscosity curves. (E) Pictures of **Ir-PH** in the mixtures of H_2O–glycerol of various viscosities under 365 nm UV light.

demonstrates that our complexes had a greater increase and a higher sensitivity for viscosity. On top of that, the lifetimes (τ) of complexes were measured in the presence of various glycerol–water mixtures. The viscosity extended gradually from 1.01 cP to 76.78 cP, and the lifetime of **Ir-PH** increased from 380 ns to 1120 ns (Fig. 2C). Furthermore, a good linear relationship was obtained between lifetime and viscosity. (Fig. 2D). At the same time, the lifetime of **Ir-PMe-2** (341–893 ns, Fig. S6C and D, ESI†) also had a linear relationship with viscosity, but its lifetime was shorter than that of **Ir-PH**. Besides, the lifetime of **Ir-PMe-1** increased from 74 ns to 406 ns, whereas lifetime–viscosity was without linear correlation (Fig. S5C and D, ESI†), unexpectedly. In general, the lifetime exhibited satisfactory specificity and sensitivity toward the viscosity. Moreover, the luminescence quantum yield (Φ) (Table S3, ESI†) and photostability (Fig. S14, ESI†) were measured.

The single crystal structures of **PH** and **Ir-PH** are shown in Fig. 1. **Ir-PH** adopted a slightly distorted octahedral geometry and four molecules make up a unit cell (Fig. S1, ESI†). The Ir–N bonds (Ir–N_{av} = 2.029 Å) of C^N ligands were shorter than the Ir–C bonds (Ir–C_{av} = 2.061 Å), while the Ir–N bonds (Ir–N_{av} = 2.133 Å) of N^N ligands were longer than the Ir–C bonds, matching with the effect of carbon donors.[30] The hexafluorophosphate would have weak interaction with C–H on two adjacent molecules (Fig. 1D). To our surprise, the torsion angles were different between ligands alone and ligands in complex (Fig. 1A–C). The torsion angle was 5.60° between the phenyl ring and purine of **PH**. While **PH** was coordinated with Ir(III), the torsion angle changed into 10.02° and 11.79°. The single crystal structure of 1-Py-βC, which is a ligand of **Ir-PH** has been reported previously,[31] and the torsion angle between the pyridine ring and β-carboline was changed from 2.31° to 20.64° before and after reacting with Ir(III). These changes may cause the tendency for the torsion angles of ligands interacting with Ir(III) to change to a single ligand's torsion angles,[32] which may explain why the **Ir-PH** has a viscosity response. Furthermore, **Ir-PMe-1** and **Ir-PMe-2** also could verify our conjecture.

In order to confirm the specificity of viscosity response of three complexes, we tested the effects of other factors on the fluorescence emission intensity of **Ir-PH**. To eliminate the calcium ion interference effect, the metal ion interference test was conducted, and no obvious changes of the emission intensity were observed (Fig. S3, ESI†). To eliminate polarity-effect, after measuring in various solvents, we carried out a fluorescence spectrum test in water-1,4-dioxane systems of different fractions (Fig. S4, ESI†), and the results revealed that there was no trend between polarity and intensity.

To utilize **Ir-PH**, **Ir-PMe-1** and **Ir-PMe-2** as a cellular viscosity sensor, we firstly investigated their cytotoxicity in A549 cells (MTS assay). As shown in Fig. S7 (ESI†), when A549 cells were treated with the three complexes at 1.25–5 μM for 24 h, a high cell viability (>90%) was obtained, which indicated that they did not interfere with the cell proliferation and physiology within the tested concentrations. After that, we desperately wanted to know whether the compounds will target the ER, so we investigated their intracellular location by a confocal microscopy experiment in cells (Fig. 3). The overlapped

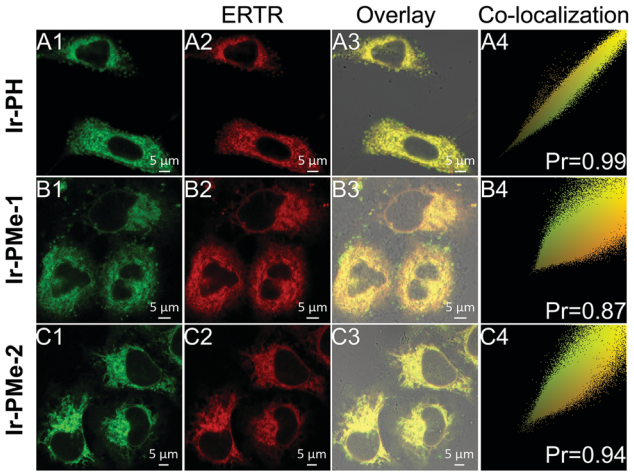

Fig. 3 (A1–A4) Confocal images of A549 cells incubated with **Ir-PH** (2 μM, λ_{ex} = 405 nm, λ_{em} = 500–600 nm) and ER-Tracker Red (500 nM, λ_{ex} = 543 nm, λ_{em} = 600–650 nm,). (B1–B4) Cellular colocalization microscopy images of A549 cells incubated with **Ir-PMe-1** (2 μM, λ_{ex} = 405 nm, λ_{em} = 500–600 nm) and ER Tracker Red (500 nM, λ_{ex} = 543 nm, λ_{em} = 600–650 nm). (C1–C4) Cellular colocalization microscopy images of A549 cells incubated with **Ir-PM-2** (2 μM, λ_{ex} = 405 nm, λ_{em} = 500–600 nm) and ER Tracker Red (500 nM, λ_{ex} = 543 nm, λ_{em} = 600–650 nm).

fluorescence image between **Ir-PH** and ER-Tracker Red demonstrated that **Ir-PH** exhibited specific ER staining and the Pearson co-localization is 0.99. On the contrary, little co-localization for **Ir-PH** with Mito-Tracker Red and Lyso-Tracker deep Red (Fig. S9, ESI†) was observed, and the co-localization values were 0.76, and 0.59, respectively. **Ir-PMe-1** and **Ir-PMe-2** had analogous results, and co-localization values of **Ir-PMe-1** were 0.90, 0.73, and 0.34 with ERTG, MTG, and LTG (Fig. S10, ESI†), respectively. Co-localization values of **Ir-PMe-2** were 0.94, 0.45, and 0.73 with ERTR, MTDR, and LTDR (Fig. S11, ESI†), respectively. These results indicated the ER-targeting ability of **Ir-PH**, **Ir-PMe-1** and **Ir-PMe-2**, especially **Ir-PH**. The excellent ER-targeting of **Ir-PH** was also confirmed in liver cancer cells (HepG 2) and liver normal cells (HL-7702) (Fig. S8, ESI†).

In order to explore the response of **Ir-PH** to ER viscosity changes, we also tested the fluorescence intensity of **Ir-PH** under ER stress in A549 cells. Tunicamycin (Tm) is a glycosylation inhibitor that obstructs the cellular biosynthesis of the N-linked oligosaccharide,[33] which is usually used to stimulate ER. As the concentration of Tm increased, the ER stimulation was more obvious, resulting in more unfolded protein and greater viscosity, and so the higher the fluorescence intensity of **Ir-PH** became (Fig. S12, ESI†), and the result was consistent with the corresponding results of *in vitro* viscosity-sensitivity tests. Besides, we also tested **Ir-PH** with Tm (50 μg mL^{-1}) at different times (Fig. S13, ESI†), and we got the same conclusion.

In our previous experiments, there was a correction between lifetime and environment viscosity of **Ir-PH**. For the purpose of monitoring the change of viscosity in ER, we used FLIM to record the results and investigated the correction *in vivo*, which may improve the drawback of images based on intensity. A seismic color scale was assigned to images Fig. 4; the blue color represented around or below 10 ns, while lifetimes

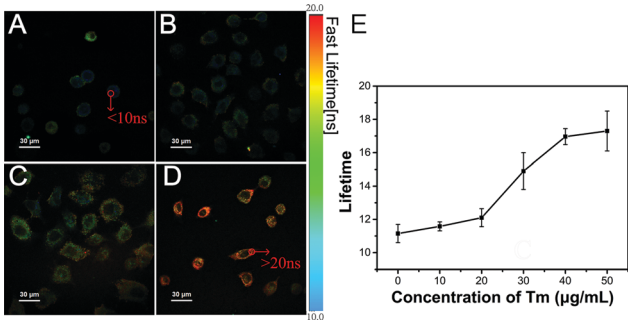

Fig. 4 FLIM of **Ir-PH** with different concentrations of Tm (A) blank; (B) 20 μg mL^{-1}; (C) 30 μg mL^{-1}; (D) 50 μg mL^{-1}; and (E) calculated lifetimes of **Ir-PH** in A549 cells.

around or above 20 ns were red. It was obvious that with the addition of Tm, the **Ir-PH** displayed slightly longer lifetimes. The calculated average fluorescence lifetime of **Ir-PH** was 11.15 ± 0.55 ns in the A549 cells with untreated Tm. With the addition of Tm, the lifetime becomes longer and longer; when the concentration of Tm was 50 μg mL^{-1}, the calculated average lifetime was 17.3 ± 1.2 ns. The lifetime of **Ir-PH** was calculated using three exponentials in A549 cells. However, the cellular environment is pretty complicated compared with water–glycerol mixtures. Therefore, **Ir-PH** might be appropriate for relative quantitative tests of ER viscosity and for the absolute quantitative detection but a standard curve was measured firstly.

In conclusion, we have designed and successfully synthesized three purine-based iridium complexes for imaging of ER. We offered an effective method to design viscosity-sensitive iridium(III) complexes by using the change of torsion angles. Between them, the fluorescence intensity and lifetime of **Ir-PH** displayed a regular response to the environmental viscosity. The subcellular localization experiment results indicated that **Ir-PH** could exclusively accumulate in the ER. Besides, due to its viscosity-sensitive lifetimes, **Ir-PH** could distinguish the changes under ER stress of cells by fluorescence lifetime image microscopy, which provides a new clue for relative quantitative detection of microenvironment changes at the subcellular level.

This work was financially supported by the National Natural Science Foundation of China (No. 22077088, and 21877082) and the Foundation from Science and Technology Department of Sichuan Province (2020JDJQ0017). We also thank Cheng-Hui Li and Peng Wu from the Analytical & Testing Center at Sichuan University for their helpful discussion about the FLIM imaging.

Conflicts of interest

There are no conflicts to declare.

Notes and references

1 A. B. Goins, H. Sanabria and M. N. Waxham, *Biophys. J.*, 2008, **95**, 5362–5373.
2 X. Liu, W. Chi, Q. Qiao, S. V. Kokate, E. P. Cabrera, Z. Xu, X. Liu and Y. Chang, *ACS Sens.*, 2020, **5**, 731–739.
3 L. Li, K. Li, M. Li, L. Shi, Y. Liu, H. Zhang, S. Pan, N. Wang, Q. Zhou and X. Yu, *Anal. Chem.*, 2018, **90**, 5873–5878.
4 W. H. Chen, G. F. Luo and X. Z. Zhang, *Adv. Mater.*, 2018, **31**, 1802725.
5 T. Hosoi and K. Ozawa, *Clin. Sci.*, 2009, **118**, 19.
6 C. Hetz, J. M. Axten and J. B. Patterson, *Nat. Chem. Biol.*, 2019, **15**, 764–775.
7 K. Bi, R. Tan, R. Hao, L. Miao, Y. He, X. Wu, J. Zhang and R. Xu, *Chin. Chem. Lett.*, 2019, **30**, 545–548.
8 S. Long, Q. Qiao, L. Miao and Z. Xu, *Chin. Chem. Lett.*, 2019, **30**, 573–576.
9 H. He, T. He, Z. Zhang, X. Xu, H. Yang, X. Qian and Y. Yang, *Chin. Chem. Lett.*, 2018, **29**, 1497–1499.
10 H. Qin, L. Li, K. Li and X. Yu, *Chin. Chem. Lett.*, 2019, **30**, 71–74.
11 K. K.-W. Lo, *Acc. Chem. Res.*, 2020, **53**, 32–44.
12 R. Zhang and J. Yuan, *Acc. Chem. Res.*, 2020, **53**, 1316–1329.
13 L. Hao, Z. Li, D. Zhang, L. He, W. Liu, J. Yang, C. Tan, L. Ji and Z. Mao, *Chem. Sci.*, 2019, **10**, 1285–1293.
14 M. Zhang, M. Wen, Y. Xiong, L. Zhang and C. Tian, *Chin. Chem. Lett.*, 2018, **29**, 1509–1512.
15 X. Li, Y. Yin, P. Gao, W. Li, H. Yan, C. Lu and Q. Zhao, *Dalton Trans.*, 2017, **46**, 13802–13810.
16 J. S. Nam, M. Kang, J. Kang, S. Park, S. J. C. Lee, H. Kim, J. K. Seo, O. Kwon, M. H. Lim, H. Rhee and T. Kwon, *J. Am. Chem. Soc.*, 2016, **138**, 10968–10977.
17 X. Li, J. Wu, L. Wang, C. He, L. Chen, Y. Jiao and C. Duan, *Angew. Chem., Int. Ed.*, 2020, **132**, 6482–6489.
18 C. Li, Y. Wang, Y. Lu, J. Guo, C. Zhu, H. He, X. Duan, M. Pan and C. Su, *Chin. Chem. Lett.*, 2020, **31**, 1183–1187.
19 C. Caporale, C. A. Bader, A. Sorvina, K. D. M. MaGee, B. W. Skelton, T. A. Gillam, P. J. Wright, P. Raiteri, S. Stagni, J. L. Morrison, S. E. Plush, D. A. Brooks and M. Massi, *Chem. – Eur. J.*, 2017, **23**, 15666–15679.
20 K. Zhang, T. Zhang, H. Wei, Q. Wu, S. Liu, Q. Zhao and W. Huang, *Chem. Sci.*, 2018, **9**, 7236–7240.
21 J. Calderón-Arancibia, C. Espinosa-Bustos, Á. Cañete-Molina, R. Tapia, M. Faúndez, M. Torres, A. Aguirre, M. Paulino and C. Salas, *Molecules*, 2015, **20**, 6808–6826.
22 C. Lambertucci, M. Buccioni, D. Dal Ben, S. Kachler, G. Marucci, A. SpinaciM, A. Thomas, K. Klotze and R. Volpini, *Med. Chem. Commun.*, 2015, **6**, 963–970.
23 M. Welsch, S. Snyder and B. Stockwell, *Curr. Opin. Chem. Biol.*, 2010, 347–361.
24 L. Shi, K. Li, L. Li, S. Chen, M. Li, Q. Zhou, N. Wang and X. Yu, *Chem. Sci.*, 2018, **9**, 8969–8974.
25 L. Shi, Y.-H. Liu, K. Li, A. Sharma, K.-K. Yu, M. Ji, L.-L. Li, Q. Zhou, H. Zhang, J. S. Kim and X.-Q. Yu, *Angew. Chem., Int. Ed.*, 2020, **59**, 9962–9966.
26 L. Shi, K. Li, Y.-H. Liu, X.-Y. Liu, Q. Zhou, Q. Xu, S.-Y. Chen and X.-Q. Yu, *Chem. Commun.*, 2020, **56**, 3661–3664.
27 P. Zhang, H. Chen, H. Huang, K. Qiu, C. Zhang, H. Chao and Q. Zhang, *Dalton Trans.*, 2019, **48**, 3990–3997.
28 F. Liu, J. Wen, S. Chen and S. Sun, *Chem. Commun.*, 2018, **54**, 1371–1374.
29 L. He, C. Tan, R. Ye, Y. Zhao, Y. Liu, Q. Zhao, L. Ji and Z. Mao, *Angew. Chem., Int. Ed.*, 2014, **53**, 12137–12141.
30 G. Li, C. Gao, H. Xie, H. Chen, D. Liu, W. Sun, G. Chen and Z. Niu, *Chin. Chem. Lett.*, 2016, **27**, 428–432.
31 C. Tan, S. Lai, S. Wu, S. Hu, L. Zhou, Y. Chen, M. Wang, Y. Zhu, W. Lian, W. Peng, L. Ji and A. Xu, *J. Med. Chem.*, 2010, **53**, 7613–7624.
32 M. J. Leitl, V. A. Krylova, P. I. Djurovich, M. E. Thompson and H. Yersin, *J. Am. Chem. Soc.*, 2014, **136**, 16032–16038.
33 D. Lee, I. Y. Kim, S. Saha and K. S. Choi, *Pharmacol. Ther.*, 2016, **162**, 120–133.

